Nuclear Inst. and Methods in Physics Research B 440 (2019) 36–40

Contents lists available at ScienceDirect

Nuclear Inst. and Methods in Physics Research B

journal homepage: www.elsevier.com/locate/nimb

Post-implantation depth profiling using time-domain Brillouin scattering

Andrey Baydin[a,*], Halina Krzyzanowska[a], Leonard Feldman[b,c], Norman Tolk[a]

[a] Department of Physics and Astronomy, Vanderbilt University, TN 37235 USA
[b] Department of Physics and Astronomy, Rutgers University, New Brunswick, NJ 08901, USA
[c] Department of Materials Science and Engineering, Rutgers University, New Brunswick, NJ 08901, USA

ARTICLE INFO

Keywords:
Ion implantation
GaAs
SiC
Diamond
Depth profiles
Refractive index
Photoelastic coefficient
Optical properties
Time domain Brillouin scattering

ABSTRACT

The unique capabilities of time domain Brillouin scattering (TDBS) for studying post-implantation effects on optical and opto-elastic properties of semiconductors are discussed. This method utilizes coherent acoustic phonons to measure depth-dependent optical and opto-elastic changes arising from structural damage caused by ion implantation. This non-destructive technique is shown to be two orders of magnitude more sensitive than Rutherford backscattering spectrometry. Results are presented for silicon carbide (SiC), gallium arsenide (GaAs) and diamond. Using the TDBS approach, we have obtained depth-dependent profiles of the complex refractive index in hydrogen implanted 4H-SiC, and of the photoelastic coefficient in hydrogen implanted GaAs. In helium implanted diamond samples, both the complex refractive index and the photoelastic coefficient have been determined. A comparison between indirect (4H-SiC, diamond) and direct (GaAs) band gap semiconductors shows the sensitivity of TDBS to the particular optical properties of different semiconductors. These studies provide basic insight into the dependence of optical properties on defect densities created by ion implantation, which is of relevance to the fabrication of photonic and optoelectronic devices. Further development of TDBS shows promise for measuring the depth dependent positions of specific defects (color centers) in wide band gap semiconductors.

1. Introduction

Essential to the basic understanding of the ion-matter interaction is the experimental determination of depth profiles of implanted species and the damage produced during the implantation process. This can provide information about the electronic and nuclear stopping mechanisms, and their coupled effects [1] involving defect dynamics [2,3]. There are various depth profiling techniques in use, e.g., Rutherford backscattering [4,5], elastic recoil detection [6,7], secondary ion mass spectrometry [8,9], particle induced X-ray emission [10,11], X-ray fluorescence [12–14], X-ray photoelectron spectroscopy [15,16], and others.

In this paper, we review advances in time-domain Brillouin scattering (TDBS) as applied to ion implanted semiconductors and show examples of depth profiling of optical and elasto-optical properties for GaAs, 4H-SiC, and diamond. TDBS, known as picosecond ultrasonics or coherent acoustic phonon (CAP) spectroscopy, is a nondestructive technique and offers markedly high depth resolution for all materials under study. It is an ultrafast optical pump–probe technique and has been thoroughly reviewed by Matsuda et al. [17] and Gusev et al. [18]. In short, an optical pump pulse absorbed in a thin transducer generates a strain wave (coherent acoustic phonons or CAP) that traverses a material. The reflection and transmission of the optical probe pulse is then modulated by the travelling CAP wave which results in a signal containing oscillations as light scatters from acoustic phonons due to Brillouin scattering. The amplitude and frequency of the Brillouin oscillations depend on the material's elastic, optical and opto-elastic properties that, in general, can be depth dependent.

To date, TDBS has been widely used to access depth dependent material properties such as elastic and optical inhomogeneities in disordered films [19–21], ion implantation induced modification of interfacial bonding [22], sub-μm textures in materials compressed at megabar pressures [23,24], doping profiles [25], depth-dependent stress [26], imaging of grain microstructure [27], and determination of laser-induced temperature gradients in liquids [28]. It has been shown that TDBS is sensitive to ion implantation induced damage in gallium arsenide [29–31], diamond [32] and silicon carbide [33] at low fluences.

2. Results

2.1. Theoretical background

The measured change in reflectivity due to propagating CAP wave (strain wave), $\eta(z, t)$, is proportional to the real part of the complex

* Corresponding author.
E-mail address: andrey.baydin@vanderbilt.edu (A. Baydin).

https://doi.org/10.1016/j.nimb.2018.11.033
Received 20 August 2018; Accepted 21 November 2018
Available online 04 December 2018
0168-583X/

reflectance, $\Delta R/R_0 = 2\mathrm{Re}[\delta r/r_0]$, where subscript zero indicates an unperturbed system. The complex reflectance for a CAP wave propagating in an inhomogeneous medium can be written as [20]:

$$\frac{\delta r(vt)}{r_0} \propto \int_0^\infty \frac{1}{k^2(z')} P_{12}(z')\eta(z', t)e^{2i\int_0^{z'} k(z)dz} dz', \quad (1)$$

where k is the wavevector, P_{12} is the photoelastic coefficient. When depth dependent variables are slowly varying functions of depth coordinate, the acoustic pulse can be assumed to be a delta-like strain pulse and integral in Eq. (1) can be taken analytically resulting in the following expression for the changes in the complex reflectance:

$$\frac{\delta r(vt)}{r_0} = \frac{C}{k^2(vt)} P_{12}(vt)e^{2i\int_0^{vt} k(z)dz}, \quad (2)$$

where v is the speed of sound, C is a complex constant. Eq. (2) is valid only when the speed of sound is constant (or its depth variation is negligible) in the damage region. This is true for all experiments presented below as they are performed in a relatively low fluence implantation regime.

2.2. Depth dependence of the photoelastic coefficient of H implanted GaAs

For direct band gap materials like GaAs, defects created by ion implantation at low fluences that cannot be measured by RBS/Channeling, affect the dielectric function and its first derivative with respect to energy (proportional to the photoelastic coefficient) [30]. Fig. 1a shows experimental data for 180 keV proton implanted GaAs at 3×10^{15} cm^{-2} probed near band edge of GaAs. Clearly, the amplitude of Brillouin oscillations is affected in the damage region while its frequency stays unchanged. This change in the amplitude then is directly related to the changes in the photoelastic coefficient arising from ion implantation. The corresponding changes in the photoelastic coefficient are plotted in Fig. 1b [31]. These changes in the photoelastic coefficient are much broader than the structural damage as predicted by the TRIM code [34]. Further analysis can be done to calibrate the technique for profiling defect concentrations as shown by Steigerwald et al. [29]. Such an approach results in measuring defect densities with higher sensitivity (two orders of magnitude) as compared to RBS/Channeling. It is important to note that TDBS requires calibration to measure defect densities directly, while RBS/Channeling does not. As for the photoelastic coefficient, TDBS is the only technique capable of measuring depth dependence of the photoelastic coefficient in a non-destructive manner. However, it only provides the relative changes in the photoelastic coefficient of the damaged sample with respect to the intrinsic material [31]. If the intrinsic value the photoelastic coefficient is not known, it can be acquired utilizing stress induced birefringence, ellipsometry under uniaxial stress, or Brillouin scattering.

2.3. Depth dependence of the complex refractive index of H implanted 4H-SiC

Silicon carbide (SiC) is an indirect wide band gap semiconductor which currently has applications in high power, high temperature, and high frequency electronic devices. This material is also being investigated for quantum information applications. TDBS experimental data for 180 keV proton irradiated n-type 4H-SiC is shown in Fig. 2 [33]. The laser wavelength was set just below the band gap (3.26 eV) at 3.1 eV. This data is very different from data shown above for GaAs. There are changes both in the amplitude and the frequency of Brillouin oscillations in the damage region. Moreover, these changes have a cumulative character, i.e. the amplitude and the phase of Brillouin oscillations is different for implanted and unimplanted specimens past the damage region. According to Eq. (2) and arguments given in the corresponding paper [33], such changes in the Brillouin oscillations can be attributed to the changes in the real and imaginary part of the complex refractive index. The depth profiles of the changes in the complex refractive index are shown in Fig. 2b,c. Remarkably, the change in the extinction coefficient is directly related (linearly) to the vacancy distribution as calculated by the TRIM code (see Fig. 2c). This suggests that this technique may be used to measure defect profiles for damage levels in SiC that are not accessible by other means. Concerning the real part of the refractive index, its profile is much broader and shows a saturation behavior with respect to vacancy concentration (see Fig. 2b). The possible reasons for such dependence are discussed in the previous paper [33]. While spectroscopic ellipsometry has been applied to measure depth profiles of the refractive index, it seems to provide lower depth resolution and it is highly sensitive to the fitting model.

2.4. Depth dependence of the complex refractive index and the photoelastic coefficient of He implanted CVD diamond

Diamond is a superior material of great interest due to its unique mechanical, electronic, thermal, and tribological properties [35]. Moreover, it hosts a wide variety of different types of color centers that are promising as quantum qubits [36–38]. Experimental data for 1 MeV He implanted single-crystal CVD diamond reported by Gregory et al.

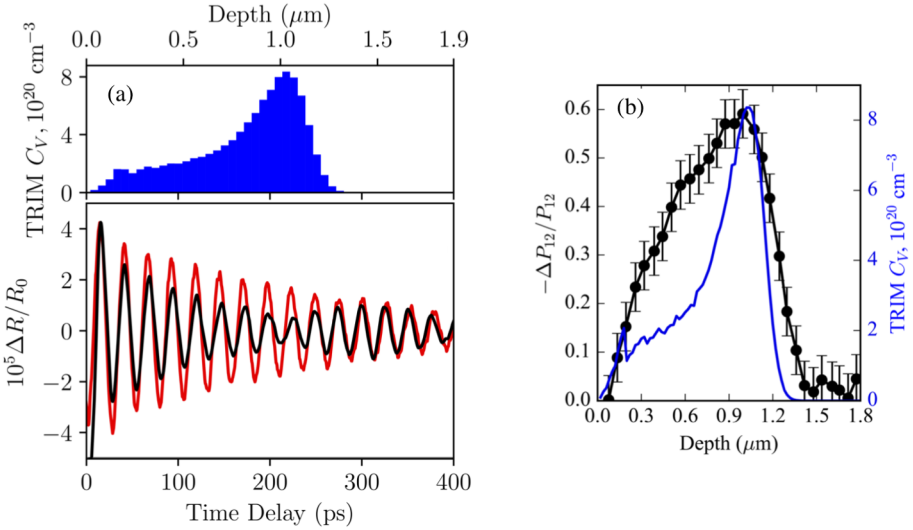

Fig. 1. (a) Damage profile as calculated by the TRIM code and Brillouin oscillations for unimplanted and implanted specimens of GaAs, (b) Depth profile of the relative changes in the photoelastic coefficient [31].

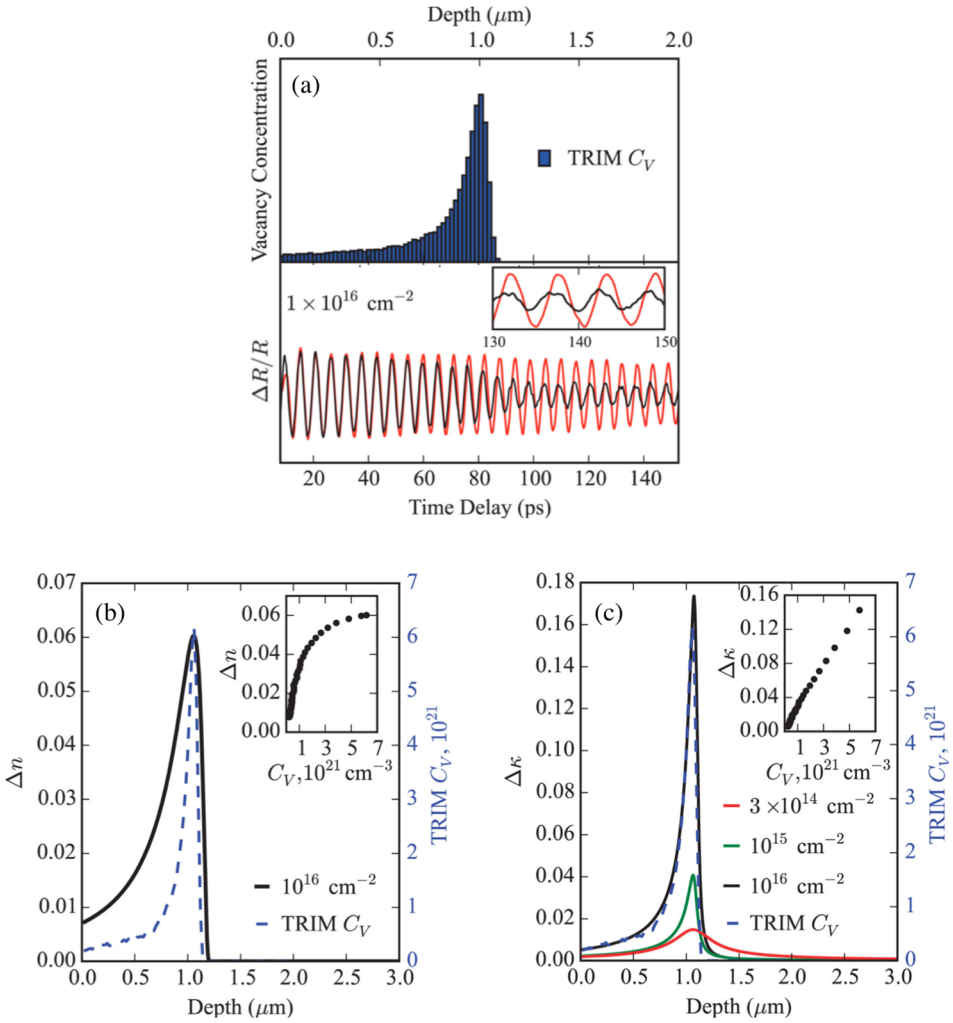

Fig. 2. (a) Damage profile as calculated by the TRIM code and Brillouin oscillations for unimplanted (red) and implanted (black) specimens of 4H-SiC. (b), (c) Depth profiles of the relative changes in the real and imaginary parts of the refractive index, respectively. Insets, show their dependence on vacancy concentration [33]. (For interpretation of the references to colour in this figure legend, the reader is referred to the web version of this article.)

[32] and shown in Fig. 3a indicates that all physical quantities (the complex refractive index and the photoelastic coefficient) vary in depth due to ion implantation induced damage. The Brillouin oscillations in this case are more complex as compared to the examples just discussed above for GaAs and 4H-SiC.

In order to fit this data, we use Eq. (2), where both the complex refractive index and the photoelastic coefficient are functions of depth coordinate. We employ a simple exponential model for the dependence of the complex refractive index on the vacancy concentration [39,40]:

$$n(C_V) = n_0 + (n_\infty - n_0)(1 - e^{-C_V/a}), \quad (3)$$

$$\kappa(C_V) = n_0 + (\kappa_\infty - \kappa_0)(1 - e^{-C_V/b}), \quad (4)$$

where n_0 and κ_0 refer to the undamaged specimen, and n_∞ and κ_∞ are saturation values for fully amorphous specimen, a and b are fitting parameters that define how optical modulation saturation is reached.

To simulate the dependence of the photoelastic coefficient on the vacancy concentration, we use the same exponential model given in Eqs. (3) and (4)

$$P_{12}(C_V) = P_{12,0} + (P_{12,\infty} - P_{12,0})(1 - e^{-C_V/c}), \quad (5)$$

where $P_{12,0}$, $P_{12,\infty}$, c are fitting parameters. C_V is the vacancy concentration and a function of depth coordinate, z. Here, the vacancy profile, , employed in the fit is the vacancy profile obtained from the TRIM code. Results of fitting procedure are shown in Fig. 3b,c,d. Interestingly, the photoelastic coefficient flips its sign in the damaged region (see Fig. 3b). Also, the profile of this coefficient is broader than the TRIM vacancy concentration profile, while the real and imaginary parts of the complex refractive index follow the TRIM vacancy concentration profile. Note, that the fitting procedure started initially with the TRIM profile which resulted in the determination of the dependence of the photoelastic coefficient and the complex refractive index on vacancy concentration. In general, the TRIM vacancy profile can be replaced by a Pearson IV function with free parameters as it was done for SiC [33]. However, the fitting approach taken here is more efficient because the fitting function has fewer free parameters. A discussion about the implications of the sign reversal of the photoelastic coefficient, the decrease in the real part of the refractive index, and the increase in the absorption coefficient (the imaginary part of the refractive index) can be found elsewhere [32,40].

3. Conclusion

In conclusion, we have reviewed recent advances in the depth profiling of optical and opto-elastic properties of ion implanted semiconductors done by time-domain Brillouin scattering. The TDBS is an all optical non-destructive technique. The different optical properties obtained by TDBS can be directly related to the structural damage, and when compared to RBS/Channeling, TDBS is two orders of magnitude more sensitive. The application of TDBS to the study of ion-matter

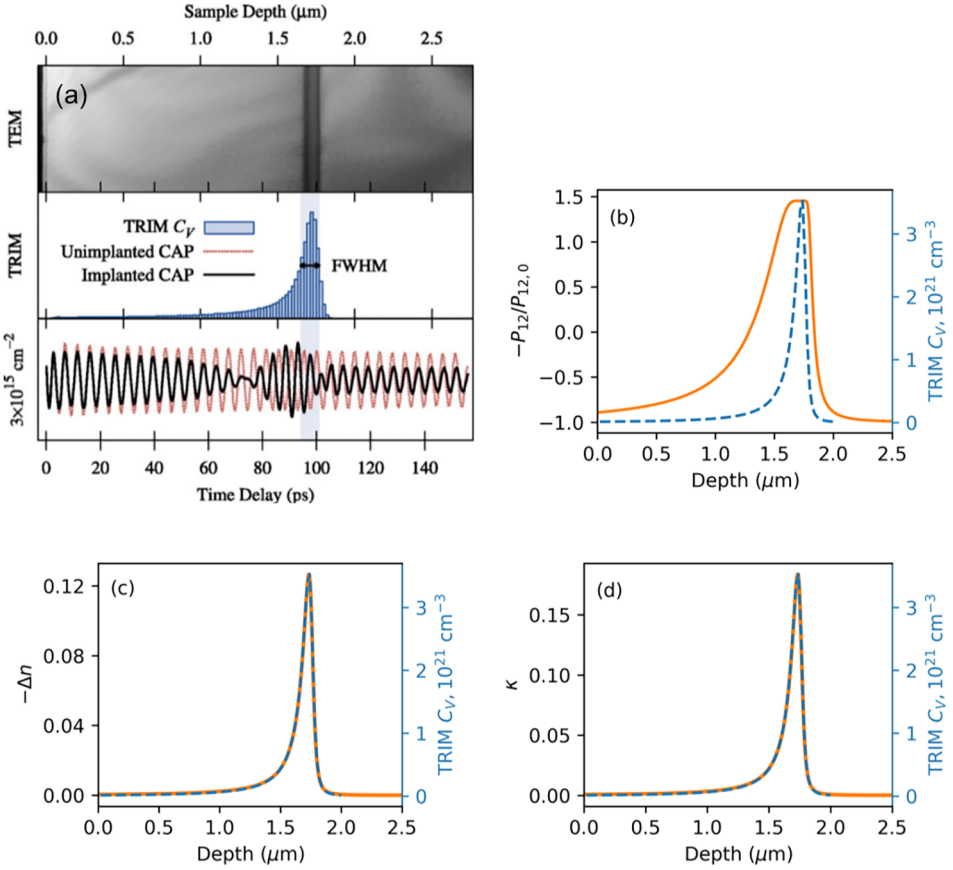

Fig. 3. (a) Transmission electron microscope cross section for 3×10^{16} cm^{-2} specimen, damage profile as calculated by the TRIM code and Brillouin oscillations for unimplanted (red) and implanted (black) specimens [32], Copyright 2012 AIP Publishing LLC. Depth profiles of the photoelastic coefficient (b), and the relative changes in the refractive index (c) and the extinction coefficient (d) for a fluence of 3×10^{15} cm^{-2} in Fig. 3a. (For interpretation of the references to colour in this figure legend, the reader is referred to the web version of this article.)

interactions is clearly advantageous in ion beam experiments over a wide range of ion fluences, in particular, where highly sensitive characterization cannot be accomplished by other means.

Acknowledgments

This work was supported by the Army Research Office [Grant No. W911NF-14-1-0290].

References

[1] Y. Zhang, H. Xue, E. Zarkadoula, R. Sachan, C. Ostrouchov, P. Liu, X.-L. Wang, S. Zhang, T.S. Wang, W.J. Weber, Coupled electronic and atomic effects on defect evolution in silicon carbide under ion irradiation, Curr. Opin. Solid State Mater. Sci. 21 (6) (2017) 285–298.
[2] L. Bayu Aji, J. Wallace, S. Kucheyev, Radiation defect dynamics in gaas studied by pulsed ion beams, J. Appl. Phys. 124 (2) (2018) 025701.
[3] L.B. Aji, J. Wallace, S. Kucheyev, Radiation defect dynamics in 3c-, 4h-, and 6h-sic studied by pulsed ion beams, Nucl. Instrum. Methods Phys. Res. Sect. B: Beam Interact. Mater. At. (2018).
[4] W.-K. Chu, J.W. Mayer, M.-A. Nicolet, Backscattering Spectroscopy, Academic Press, New York, 1978.
[5] L.C. Feldman, J.W. Mayer, S.T. Picraux, Materials Analysis by Ion Channeling: Submicron Crystallography, Academic Press, 2012.
[6] W.A. Bik, F. Habraken, Elastic recoil detection, Rep. Prog. Phys. 56 (7) (1993) 859.
[7] Y. Serruys, J. Tirira, P. Trocellier, Forward Recoil Spectrometry: Applications to Hydrogen Determination in Solids, Springer Science & Business Media, 2012.
[8] J. Griffiths, Secondary ion mass spectrometry, Anal. Chem. 80 (19) (2008) 7194–7197.
[9] A. Benninghoven, F. Rudenauer, H.W. Werner, Secondary ion mass spectrometry: basic concepts, instrumental aspects, applications and trends.
[10] S.A. Johansson, T.B. Johansson, Analytical application of particle induced X-ray emission, Nucl. Instrum. Methods 137 (3) (1976) 473–516.
[11] S.A. Johansson, J.L. Campbell, K.G. Malmqvist, J.D. Winefordner, et al., Particle-induced X-ray emission spectrometry (PIXE) Vol. 133 John Wiley & Sons, 1995.
[12] R. Jenkins, X-ray fluorescence spectrometry, Ullmann's Encyclopedia of Industrial Chemistry.
[13] V. Thomsen, Basic fundamental parameters in X-ray fluorescence, Spectroscopy 22 (5) (2007) 46–50.
[14] H. Krzyżanowska, A. von Bohlen, R. Klockenkämper, Depth profiles of shallow implanted layers by soft ion sputtering and total-reflection X-ray fluorescence, Spectrochim. Acta Part B: At. Spectrosc. 58 (12) (2003) 2059–2067.
[15] G. Friedbacher, H. Bubert, Surface and Thin Film Analysis: A Compendium of Principles, Instrumentation, and Applications, John Wiley & Sons, 2011.
[16] J. Żuk, H. Krzyżanowska, M. Clouter, M. Bromberek, H. Bubert, L. Rebohle, W. Skorupa, Brillouin scattering and X-ray photoelectron studies of germanium nanoclusters synthesized in si o 2 by ion implantation, J. Appl. Phys. 96 (9) (2004) 4952–4959.
[17] O. Matsuda, M.C. Larciprete, R. Li Voti, O.B. Wright, Fundamentals of picosecond laser ultrasonics, Ultrasonics 56 (2015) 3, https://doi.org/10.1016/j.ultras.2014.06.005.
[18] V.E. Gusev, P. Ruello, Advances in applications of time-domain Brillouin scattering for nanoscale imaging, Appl. Phys. Rev. 5 (3) (2018) 031101, https://doi.org/10.1063/1.5017241.
[19] C. Mechri, P. Ruello, J.M. Breteau, M.R. Baklanov, P. Verdonck, V. Gusev, Depth-profiling of elastic inhomogeneities in transparent nanoporous low-k materials by picosecond ultrasonic interferometry, Appl. Phys. Lett. 95 (9) (2009) 091907, https://doi.org/10.1063/1.3220063.
[20] V. Gusev, A.M. Lomonosov, P. Ruello, A. Ayouch, G. Vaudel, Depth-profiling of elastic and optical inhomogeneities in transparent materials by picosecond ultrasonic interferometry: theory, J. Appl. Phys. 110 (12) (2011) 124908, https://doi.org/10.1063/1.3665646.
[21] A.M. Lomonosov, A. Ayouch, P. Ruello, G. Vaudel, M.R. Baklanov, P. Verdonck, L. Zhao, V.E. Gusev, Nanoscale noncontact subsurface investigations of mechanical and optical properties of nanoporous low-k material thin film, ACS Nano 6 (2) (2012) 1410, https://doi.org/10.1021/nn204210u.
[22] G. Tas, J.J. Loomis, H.J. Maris, A.A. Bailes, L.E. Seiberling, Picosecond ultrasonics study of the modification of interfacial bonding by ion implantation, Appl. Phys. Lett. 72 (18) (1998) 2235, https://doi.org/10.1063/1.121276.
[23] S.M. Nikitin, N. Chigarev, V. Tournat, A. Bulou, D. Gasteau, B. Castagnede, A. Zerr, V.E. Gusev, Revealing sub-μm and μm-scale textures in H2O ice at megabar pressures by time-domain Brillouin scattering, Sci. Rep. 5 (1) (2015) 9352, https://doi.org/10.1038/srep09352.

[24] M. Kuriakose, S. Raetz, N. Chigarev, S.M. Nikitin, A. Bulou, D. Gasteau, V. Tournat, B. Castagnede, A. Zerr, V.E. Gusev, Picosecond laser ultrasonics for imaging of transparent polycrystalline materials compressed to megabar pressures, Ultrasonics 69 (2016) 259, https://doi.org/10.1016/j.ultras.2016.03.007.
[25] F. Hudert, A. Bartels, T. Dekorsy, K. Köhler, Influence of doping profiles on coherent acoustic phonon detection and generation in semiconductors, J. Appl. Phys. 104 (2008) 123509, https://doi.org/10.1063/1.3033140.
[26] J. Dai, P. Mukundhan, C. Kim, H.J. Maris, Analysis of a picosecond ultrasonic method for measurement of stress in a substrate, J. Appl. Phys. 119 (10) (2016) 105705, https://doi.org/10.1063/1.4943541.
[27] M. Khafizov, J. Pakarinen, L. He, H. Henderson, M. Manuel, A. Nelson, B. Jaques, D. Butt, D. Hurley, Subsurface imaging of grain microstructure using picosecond ultrasonics, Acta Mater. 112 (2016) 209, https://doi.org/10.1016/j.actamat.2016.04.003.
[28] I. Chaban, D. Shin, C. Klieber, R. Busselez, V. Gusev, K.A. Nelson, T. Pezeril, Time-domain Brillouin scattering for the determination of laser-induced temperature gradients in liquids, Rev. Sci. Instrum. 88 (2017) 074904, https://doi.org/10.1063/1.4993132.
[29] A. Steigerwald, Y. Xu, J. Qi, J. Gregory, X. Liu, J.K. Furdyna, K. Varga, a.B. Hmelo, G. Lüpke, L.C. Feldman, N. Tolk, Semiconductor point defect concentration profiles measured using coherent acoustic phonon waves, Appl. Phys. Lett. 94 (11) (2009) 111910, https://doi.org/10.1063/1.3099341.
[30] A. Steigerwald, A.B. Hmelo, K. Varga, L.C. Feldman, N. Tolk, Determination of optical damage cross-sections and volumes surrounding ion bombardment tracks in GaAs using coherent acoustic phonon spectroscopy, J. Appl. Phys. 112 (1) (2012) 013514, https://doi.org/10.1063/1.4732072.
[31] A. Baydin, H. Krzyzanowska, R. Gatamov, J. Garnett, N. Tolk, The photoelastic coefficient P 12 of H+ implanted GaAs as a function of defect density, Scientific Reports 7 (1) (2017) 15150, https://doi.org/10.1038/s41598-017-14903-x.
[32] J. Gregory, A. Steigerwald, H. Takahashi, A. Hmelo, N. Tolk, Ion implantation induced modification of optical properties in single-crystal diamond studied by coherent acoustic phonon spectroscopy, Appl. Phys. Lett. 101 (18) (2012) 181904, https://doi.org/10.1063/1.4765647.
[33] A. Baydin, H. Krzyzanowska, M. Dhanunjaya, S.V.S.N. Rao, J.L. Davidson, L.C. Feldman, N.H. Tolk, Depth dependent modification of optical constants arising from H+ implantation in n-type 4H-SiC measured using coherent acoustic phonons, APL Photonics 1 (3) (2016) 036102, https://doi.org/10.1063/1.4945443.
[34] J.F. Ziegler, M. Ziegler, J. Biersack, SRIM – the stopping and range of ions in matter (2010), Nucl. Instrum. Methods Phys. Res., Sect. B 268 (11–12) (2010) 1818, https://doi.org/10.1016/j.nimb.2010.02.091.
[35] J.E. Field, J.E. Field, The Properties of Diamond, Academic Press, 1979.
[36] G. Fuchs, G. Burkard, P. Klimov, D. Awschalom, A quantum memory intrinsic to single nitrogen-vacancy centres in diamond, Nat. Phys. 7 (10) (2011) 789–793.
[37] S. Pezzagna, D. Rogalla, D. Wildanger, J. Meijer, A. Zaitsev, Creation and nature of optical centres in diamond for single-photon emission–overview and critical remarks, New J. Phys. 13 (3) (2011) 035024 .
[38] F. Waldermann, P. Olivero, J. Nunn, K. Surmacz, Z. Wang, D. Jaksch, R. Taylor, I. Walmsley, M. Draganski, P. Reichart, et al., Creating diamond color centers for quantum optical applications, Diam. Relat. Mater. 16 (11) (2007) 1887–1895.
[39] A. Battiato, F. Bosia, S. Ferrari, P. Olivero, A. Sytchkova, E. Vittone, Spectroscopic measurement of the refractive index of ion-implanted diamond, Opt. Lett. 37 (4) (2012) 671–673.
[40] J.M. Gregory, Effect of Electron and Phonon Excitation on the Optical Properties of Indirect Gap Semiconductors, Vanderbilt University, 2013.